East European Journal of Physics. 2. 19–33 (2026)
DOI: 10.26565/2312-4334-2026-2-02 ISSN 2312-4334

CONSTRAINING KANIADAKIS HOLOGRAPHIC DARK ENERGY MODEL IN BIANCHI TYPE–*III* COSMOLOGY

Y. Aditya[1*], **K. Dasunaidu**[1**], **Muralasetti Nookaraju**[2], **P. Silpa**[3], **G. Suryanarayana**[4]
[1]*Department of Mathematics, GMR Institute of Technology (GMRIT) – Deemed to be University, Rajam-532127, India*
[2]*Department of Chemistry, Aditya University, Surampalem-533437, India*
[3]*Department of Chemistry, Sri Vasavi Engineering College, Tadepalligudem-534101, India*
[4]*Department of Mathematics, ANITS, Visakhapatnam-533003, India*
[*]*Corresponding Author e-mail: [*]aditya.y@gmrit.edu.in; [**]dasunaidu.k@gmrit.edu.in*
Received February 6, 2026; revised April 21, 2026; accepted May 6, 2026

In this work, we study the cosmological dynamics of an anisotropic Bianchi type–*III* universe filled with Kaniadakis holographic dark energy and pressureless matter within the framework of Brans–Dicke–Rastall theory of gravity. To obtain exact solutions of the field equations, suitable relations among the metric potentials are assumed, together with a functional relation between the scalar field and the average scale factor. To constrain the model parameters, we perform a Markov Chain Monte Carlo analysis using joint CC+BAO datasets. The reconstructed Hubble parameter shows excellent agreement with observational data within the 1σ and 2σ confidence regions, and the estimated value of the Hubble constant is consistent with recent measurements. We derive several important cosmological parameters, including the Hubble parameter, deceleration parameter, equation of state parameter, scalar field, cosmic time and lookback time. The physical behavior of these parameters is analyzed through graphical representations. The deceleration parameter exhibits a smooth transition from an early decelerated phase to a late–time accelerated phase, with a transition redshift consistent with recent observational bounds. The equation of state parameter remains in the phantom region, indicating a dynamical dark energy behavior capable of driving the current accelerated expansion. Furthermore, the statefinder (r, s) and (r, q) diagnostics reveal that the model closely approaches the ΛCDM behavior at late times, while allowing deviations at earlier epochs. The $Om(z)$ diagnostic further supports the phantom–like nature of dark energy in the present framework. Overall, our results demonstrate that our model in Brans–Dicke–Rastall gravity provides a viable and observationally consistent description of the cosmic expansion history in an anisotropic universe.

Keywords: *Kaniadakis holographic dark energy; Brans–Dicke–Rastall gravity; Bianchi type–III universe; MCMC analysis; Cosmic acceleration*

PACS: 98.80.-k, 04.50.+h, 95.30.Sf

1. INTRODUCTION

Recent technological developments have led to a new era known as precision cosmology, where the large–scale properties of the Universe can be measured with high accuracy [1]. Even with these improvements, most of the Universe is still not fully understood. Observations such as galaxy rotation curves, gravitational lensing, and large–scale surveys confirm the presence of dark matter, which makes up nearly 25% of the total energy content of the Universe [2]. An even bigger mystery is dark energy (DE), which contributes about 70% of the present energy density and is responsible for the accelerated expansion of the Universe. Although strong evidence for DE comes from gravitational waves, baryon acoustic oscillations, and Type Ia supernova observations, its true nature is still unknown [3, 4]. This suggests that new physics beyond the standard model may be needed. One approach is modified gravity, where Einstein's general relativity is extended by adding new terms or scalar fields [5, 6]. A well–known example is the Brans–Dicke theory, where the gravitational constant G is replaced by a changing scalar field ϕ ($G^{-1} = \phi$) [7, 8]. Although this theory can explain cosmic acceleration, its predicted parameters often disagree with observations, so additional dark energy models are usually considered [9, 10, 11].

The cosmological constant was initially regarded as the simplest explanation for dark energy, since it represents vacuum energy and naturally produces accelerated cosmic expansion. Nevertheless, this interpretation faces well–known theoretical difficulties, notably the fine–tuning and coincidence problems. Motivated by these issues, the Holographic Dark Energy (HDE) model emerged as an alternative framework inspired by the holographic principle [12, 13]. The original HDE formulation is based on the Bekenstein–Hawking entropy relation and commonly adopts the Hubble horizon as the infrared (IR) cutoff, providing a quantitative description of dark energy. However, the standard HDE model struggles to fully describe the complete evolutionary history of a flat Friedmann–Robertson–Walker (FRW) Universe. To address these shortcomings, several extensions have been proposed, including the use of alternative IR cutoffs [14] and the introduction of interactions between dark energy and dark matter [15]. More recently, modified HDE models based on entropy–area law deformations have been developed while still employing the Hubble radius as the IR cutoff [16, 17, 18]. Such

Cite as: Y. Aditya, K. Dasunaidu, Muralasetti Nookaraju, P. Silpa, G. Suryanarayana, East Eur. J. Phys. 2, 19 (2026), https://doi.org/10.26565/2312-4334-2026-2-02

generalized models aim to provide a more flexible and observationally compatible explanation of cosmic acceleration. Further progress has been achieved through the introduction of generalized entropy formalisms, including Tsallis [19], Sharma–Mittal [20], and Rényi [21] entropies, to extend the HDE scenario. A significant unifying approach was proposed by Nojiri et al. [22, 23, 24], who introduced a four–parameter generalized entropy encompassing several well–known entropy measures as limiting cases. Among these, the Kaniadakis entropy [25] stands out as a one–parameter deformation of Boltzmann–Gibbs entropy, particularly suitable for strong gravitational regimes [26, 27]. Its incorporation into HDE leads to the Kaniadakis holographic dark energy (KHDE) model [28], which offers enhanced flexibility and potential solutions to long–standing cosmological problems such as fine–tuning and cosmic coincidence.

Rastall's theory of gravity is a non–Lagrangian modification of General Relativity in which the usual conservation of the energy–momentum tensor is relaxed. In Einstein's theory, the divergence of the energy–momentum tensor vanishes due to the divergence–free property of the Einstein tensor. Rastall proposed that in curved space–time the standard conservation law $T^{ij}_{\ ;i} = 0$ may not strictly apply and allowed a non–zero divergence instead [29]. The deviation from standard conservation is controlled by a dimensionless parameter λ, representing a non–minimal coupling between matter and geometry. This idea is physically motivated by cosmological particle creation processes, where classical conservation laws may effectively break down. In this sense, Rastall gravity can be viewed as a classical description that mimics certain quantum effects, since the non–conservation of the energy–momentum tensor is linked to space–time curvature [30, 31]. Similar relaxations of conservation laws have also inspired alternative Lagrangian approaches [32, 33]. The equivalence between Rastall gravity and General Relativity remains debated: some studies treat it as a genuine modification [34], while others argue for mathematical equivalence under specific conditions [35]. Recent works further examine its cosmological and dynamical implications [36, 37].

Rastall Theory: Since the formulation of general relativity, several alternative geometric theories of gravity have been proposed to better understand gravitational phenomena and cosmological evolution (see, for example, Rastall [29]; Brans and Dicke [8]; Moffat [38]; and Bekenstein [39]). A fundamental feature of GR is the conservation of the energy–momentum tensor. One of the earliest attempts to relax this conservation principle appeared in the steady–state cosmological model proposed by Bondi and Gold [40] and Hoyle [41]. Building on this idea, Rastall introduced a non–conservative theory of gravity by modifying the usual conservation law to $T^{ij}{}_{;i} = kR^{;j}$, where T^{ij} is the energy–momentum tensor, R is the Ricci scalar curvature, and k is a coupling constant. This modification implies that particle creation processes in cosmology may lead to an effective violation of classical conservation laws, with the deviation being directly related to the curvature of space–time. In this framework, the geometry and matter fields are non–minimally coupled, leading to a generalized form of Einstein's field equations. Rastall's modified gravitational field equations can be written as $G_{ij} + \lambda g_{ij} R = \kappa T_{ij}$, where λ is the Rastall parameter measuring the departure from standard conservation and κ is the gravitational coupling constant.

$$R_{ij} - \frac{1}{2} g_{ij} R = 8\pi G \left(T_{ij} - \frac{\lambda_{Ras} - 1}{2} g_{ij} T \right) \tag{1}$$

with equation of motion

$$T^{ij}_{\ ;i} = \frac{\lambda_{Ras} - 1}{2} T^{;j} \tag{2}$$

where $T^{ij}_{\ ;i} = \frac{\lambda_{Ras}-1}{16\pi G(2\lambda_{Ras}-3)} R^{;j}$ or $T^{ij}_{\ ;i} = \frac{\lambda_{Ras}-1}{2} T^{;j}$ with $R = 8\pi G(2\lambda_{Ras} - 3)T$, T is the trace of the stress-energy momentum tensor, and λ_{Ras} is Rastall's parameter. One can recover GR field equations by setting $\lambda_{Ras} = 1$.

Brans-Dicke-Rastall Theory: In the BD context, identifying $G = \frac{1}{\phi}$ and $\lambda_{Ras} = \frac{3\lambda-2}{2\lambda-1}$, λ is BDR parameter, in Eq. (2), we obtain the following relation:

$$T^{ij}_{\ ;i} = \frac{(1-\lambda)\phi}{16\pi} R^{;j}. \tag{3}$$

Generalizing Rastall's field equations to the BD case, we obtain:

$$R_{ij} - \frac{\lambda}{2} g_{ij} R = \frac{8\pi}{\phi} T_{ij} + \left(-\frac{1}{2} g_{ij} \phi_{;k} \phi^{;k} + \phi_{;i} \phi_{;j} \right) \frac{w}{\phi^2} + \frac{1}{\phi} \left(-g_{ij} \Box\phi + \phi_{;i;j} \right) \tag{4}$$

in which the dimensionless BD coupling parameter is denoted by w and the BD scalar field is denoted by ϕ. The trace of the Eq. (4) is obtained as

$$R = \frac{1}{1-2\lambda} \left(\frac{8\pi}{\phi} T - \frac{w}{\phi^2} \phi_{;k} \phi^{;k} - 3\frac{\Box\phi}{\phi} \right). \tag{5}$$

Now, using the Eqs. (4) and (5), we obtain the BDR theory field equations as

$$R_{ij} - \frac{1}{2} g_{ij} R = \frac{8\pi}{\phi} \left(T_{ij} - \frac{1-\lambda}{2(1-2\lambda)} g_{ij} T \right) + \left(\frac{\lambda}{2(1-2\lambda)} g_{ij} \phi_{;k} \phi^{;k} + \phi_{;i} \phi_{;j} \right) \frac{w}{\phi^2}$$

$$+\frac{1}{\phi}\left(\frac{1+\lambda}{2(1-2\lambda)}g_{ij}\Box\phi+\phi_{;i;j}\right). \tag{6}$$

The Bianchi identities lead to:

$$\Box\phi=\frac{8\pi\lambda}{3\lambda-2(1-2\lambda)w}T-\frac{w(1-\lambda)}{3\lambda-2(1-2\lambda)w}\frac{\phi^{;k}\phi_{;k}}{\phi}. \tag{7}$$

For $\lambda = 1$, the Brans–Dicke–Rastall (BDR) theory reduces to the standard BD model. BDR is distinctive because it unifies scalar–tensor dynamics with a non–conservative energy–momentum framework inspired by Rastall gravity. Unlike higher–order theories such as $f(R)$ gravity, BDR preserves second–order field equations and involves fewer dynamical degrees of freedom, making it mathematically simpler. The additional parameters λ and ω provide flexibility for fitting cosmological observations and explaining late–time cosmic acceleration. Its non–conservative nature allows effective matter creation or matter–geometry interaction, enabling the model to mimic dark energy effects and slightly modify astrophysical structures compared to GR or BD theory.

The choice of a Bianchi type (BT)-III background allows for the incorporation of spatial anisotropy, which may have been significant in the early universe (Ref. [42]-[52]). While current cosmological observations strongly support isotropy on large scales, considering anisotropic geometries like BT-III offers deeper insights into possible deviations from perfect isotropy and helps to understand how anisotropies might decay or leave imprints on late-time cosmic dynamics. Studies on KHDE are also emerging in various contexts [53, 54, 55, 56]. Ghaffari [57] studied KHDE model in BD theory of gravity and investigated their cosmological consequences. Ali et al. [58] explored the dynamics of isotropic KHDE model in the Chern-Simons modified theory. Murali et al. [59, 60] have investigated anisotropic KHDE models in scalar-tensor theory of gravity. Embedding these two aspects of the universe in the background of BDR theory further enhances its physical relevance. BD gravity introduces a dynamical scalar field, reflecting Mach's principle and varying gravitational coupling, while Rastall's hypothesis modifies the conservation law of the energy–momentum tensor. Their combination (i.e., BDR theory) provides an effective platform to explore non-standard energy exchange between matter, geometry, and DE, which is crucial for explaining cosmic acceleration without relying exclusively on a cosmological constant. The Hubble cutoff provides a simple and large-scale measure of cosmic dynamics. With this motive, the investigation of BT-III KHDE model with Hubble cutoff within the framework of BDR theory provides a promising way to address fundamental questions about the universe's accelerated expansion and the role of extended theories of gravity. We organized the paper as follows: Section-2 consists the field equations of the model and analytical solution of the field equations. Section-3 includes the observational constraints made on these solutions are imposed by cosmic chronometer and BAO Hubble datasets using Markov Chain Monte Carlo analysis. In section-4, we discuss the dynamical behavior of models, and conclusions are given in section-5.

2. KANIADAKIS HOLOGRAPHIC DARK ENERGY MODEL

The BT–III space–time is considered in the following form:

$$ds^2=dt^2-[A(t)]^2dx^2-[B(t)]^2e^{2x}dy^2-[C(t)]^2dz^2. \tag{8}$$

From the non–vanishing components of the Einstein tensor for the BT–III space–time, it is observed that $G_4^1=\frac{\dot{A}}{A}-\frac{\dot{B}}{B}=0$, which, upon integration, yields the relation $A=a_1B$, where a_1 is an integration constant. Without loss of generality, by choosing $a_1=1$, we obtain $A=B$. The total energy–momentum tensor of the source is assumed to be a combination of the matter and dark energy components (in mixed form), $T_i^{j(tot)}=T_i^{j(m)}+T_i^{j(de)}$. We define the matter and DE tensors as diagonal tensors in the comoving frame (i.e., $u^i=(1,0,0,0)$, $u_i=(1,0,0,0)$ and $u^iu_i=1$), namely

$$T_i^{j(m)}=\mathrm{diag}(\rho_m,\,0,\,0,\,0)\,,\qquad \overline{T}_i^{j(de)}=\mathrm{diag}\big(\rho_{de},\,-p_x,\,-p_y,\,-p_z\big)\,, \tag{9}$$

with the anisotropic equation of state

$$p_x=\omega_{de}\rho_{de},\qquad p_y=\omega_{de}\rho_{de},\qquad p_z=(\omega_{de}+\gamma)\rho_{de}, \tag{10}$$

where the EoS parameter ω_{de} and the energy densities of matter are denoted as ρ_m and DE as ρ_{de} in this equation. The deviation parameter, γ, is the deviation along z-direction from the EoS parameter.

The BDR field equations (6) for the metric (8) in a comoving coordinate system can be formally expressed using (9) and (10) as

$$\begin{aligned}\frac{\ddot{A}}{A}+\frac{\ddot{C}}{C}+\frac{\dot{A}\dot{C}}{AC} &= \frac{8\pi}{\phi}\left(\frac{1+\lambda}{2-4\lambda}\omega_{de}\rho_{de}+\frac{1-\lambda}{2-4\lambda}\gamma\rho_{de}+\frac{\lambda-1}{2-4\lambda}(\rho_m+\rho_{de})\right)+w\left(\frac{\dot{\phi}}{\phi}\right)^2\left(\frac{\lambda}{2-4\lambda}\right)\\ &\quad+\left(\frac{2-\lambda}{1-2\lambda}\right)\frac{\dot{A}}{A}\frac{\dot{\phi}}{\phi}+\left(\frac{1+\lambda}{2-4\lambda}\right)\frac{\dot{C}}{C}\frac{\dot{\phi}}{\phi}+\left(\frac{1+\lambda}{2-4\lambda}\right)\frac{\ddot{\phi}}{\phi}\end{aligned} \tag{11}$$

$$2\frac{\ddot{A}}{A}+\left(\frac{\dot{A}}{A}\right)^2-\frac{1}{A^2} = \frac{8\pi}{\phi}\left(\frac{1+\lambda}{2-4\lambda}\omega_{de}\rho_{de}+\frac{3\lambda-1}{2-4\lambda}\gamma\rho_{de}+\frac{\lambda-1}{2-4\lambda}(\rho_m+\rho_{de})\right)+w\left(\frac{\dot{\phi}}{\phi}\right)^2\left(\frac{\lambda}{2-4\lambda}\right) + \left(\frac{1+\lambda}{1-2\lambda}\right)\frac{\dot{A}}{A}\frac{\dot{\phi}}{\phi}+\left(\frac{3-3\lambda}{2-4\lambda}\right)\frac{\dot{C}}{C}\frac{\dot{\phi}}{\phi}+\left(\frac{1+\lambda}{2-4\lambda}\right)\frac{\ddot{\phi}}{\phi} \tag{12}$$

$$2\frac{\dot{A}}{A}\frac{\dot{C}}{C}+\left(\frac{\dot{A}}{A}\right)^2-\frac{1}{A^2} = \frac{8\pi}{\phi}\left(\frac{1-3\lambda}{2-4\lambda}(\rho_m+\rho_{de})+\frac{3-3\lambda}{2-4\lambda}\omega_{de}\rho_{de}+\frac{1-\lambda}{2-4\lambda}\gamma\rho_{de}\right) +w\left(\frac{\dot{\phi}}{\phi}\right)^2\left(\frac{2-3\lambda}{2-4\lambda}\right)+\left(\frac{1+\lambda}{1-2\lambda}\right)\frac{\dot{A}}{A}\frac{\dot{\phi}}{\phi}+\left(\frac{1+\lambda}{2-4\lambda}\right)\frac{\dot{C}}{C}\frac{\dot{\phi}}{\phi} +\left(\frac{3-3\lambda}{2-4\lambda}\right)\frac{\ddot{\phi}}{\phi} \tag{13}$$

$$\ddot{\phi}+\left(\frac{2\dot{A}}{A}+\frac{\dot{C}}{C}\right)\dot{\phi}=\left(\frac{8\pi\lambda(\rho_{de}+\rho_m-3\omega_{de}\rho_{de}-\gamma\rho_{de})}{3\lambda-2(1-2\lambda)w}\right)-\left(\frac{w(1-\lambda)}{3\lambda-2(1-2\lambda)w}\right)\left(\frac{\dot{\phi}^2}{\phi}\right). \tag{14}$$

The field equations given in Eqs. (11)–(14) constitute a system of four independent equations containing six unknown functions, namely the metric potentials A and C, the dark energy density ρ_{de}, its equation of state parameter ω_{de}, the matter density ρ_m, and the skewness parameter γ. To obtain a deterministic solution, two additional physically motivated constraints are required. A commonly adopted assumption is that the expansion scalar $\theta=\frac{2\dot{A}}{A}+\frac{\dot{C}}{C}$ is proportional to the shear scalar $\sigma^2=\frac{1}{3}\left(\frac{\dot{A}}{A}-\frac{\dot{C}}{C}\right)^2$, which leads to a simple relation between the metric potentials of the form $C=A^k$, where $k\neq 1$ is an arbitrary constant. The physical relevance of this proportionality condition has been discussed in detail by Thorne [61]. Observational evidence indicates that the present Hubble expansion of the Universe is nearly isotropic within approximately ±30% [62, 63], and measurements at moderate redshifts further constrain the ratio $\sigma/H\leq 0.3$. The assumption that σ/H remains constant corresponds to a normal congruence, as shown by Collins et al. [64], and is valid for spatially homogeneous space–times. In addition, following common practice in the literature, we assume a power–law relation between the scalar field and the scale factor, $\phi\propto[a(t)]^n$, which has been widely employed in scalar–tensor cosmological studies [65, 66]. Several investigations have examined the dynamical behavior of the scalar field under this assumption [67]-[70]. Motivated by its physical significance and its ability to simplify the system, we adopt the relation $\phi(t)=\phi_0[a(t)]^k$, where ϕ_0 is a constant of proportionality.

Using the above relations in Eqs. (12) and (13), we get

$$\frac{\ddot{A}}{\dot{A}}+\left(\frac{3k+3+kn+2n}{3}\right)\frac{\dot{A}}{A}=\frac{1}{k-1}\left[\frac{8\pi\gamma\rho_{de}}{\phi}-\frac{1}{A^2}\right]\frac{A}{\dot{A}} \tag{15}$$

The relationship between DE's energy density and the skewness or deviation parameter has been the subject of numerous recent investigations. Anisotropic DE models were investigated by Akarsu and Kilinc [71], who took into account a correlation between DE energy density and skewness factors. In a similar vein, Sharif and Zubair [72] examined dynamical anisotropic DE models using the identical relation. We assume the following relationship between $\gamma(t)$ and ρ_{de} in order to completely resolve Eq. (15)

$$\gamma(t)=\frac{\phi}{8\pi\rho_{de}}\left[(k-1)\gamma_0\frac{\dot{A}}{A}+\frac{1}{A^2}\right] \tag{16}$$

in which every given constant is represented by γ_0. Various authors have explored comparable relationships in the literature [73]-[76]. We can find our model's metric potentials by plugging the Eq. (16) into Eq. (15)

$$A = \left(k_1e^{\gamma_0t}+k_2\right)^{\frac{b_2}{k_2}},\quad C=\left(k_1e^{\gamma_0t}+k_2\right)^{\frac{kb_2}{k_2}} \tag{17}$$

where $k_1=\frac{(k+2)(n+3)}{3}\frac{b_1}{\gamma_0}$, $k_2=\frac{(k+2)b_2(n+3)}{3}$, b_1 and b_2 are integrating constants. Now using these metric potentials (17), we can rewrite the space-time as

$$ds^2=dt^2-\left(k_1e^{\gamma_0t}+k_2\right)^{\frac{2b_2}{k_2}}dx^2-\left(k_1e^{\gamma_0t}+k_2\right)^{\frac{2b_2}{k_2}}e^{2x}dy^2-\left(k_1e^{\gamma_0t}+k_2\right)^{\frac{2kb_2}{k_2}}dz^2. \tag{18}$$

Now the scalar field ϕ calculated as

$$\phi=\phi_0\left(k_1e^{\gamma_0t}+k_2\right)^{\frac{n}{n+3}}. \tag{19}$$

The Hubble parameter $H(z)$ can be obtained as

$$H = \frac{1}{3}\left(2\frac{\dot{A}}{A} + \frac{\dot{C}}{C}\right) = \left(\frac{k+2}{3}\right)\left(\frac{b_2}{k_2}\right)\left(\frac{k_1 e^{\gamma_0 t}\gamma_0}{k_1 e^{\gamma_0 t} + k_2}\right) \tag{20}$$

$$= \frac{\gamma_0}{n+3}\left[1 - k_2(1+z)^{n+3}\right]$$

$$= \frac{H_0}{1-k_2}\left(1 - k_2(1+z)^{n+3}\right) \tag{21}$$

where $1 + z = \frac{1}{a(t)}$ and $a(t)$ is average scale factor. Here $\frac{H_0}{1-k_2} = \frac{\gamma_0}{n+3}$. We will constrain following parameters H_0, n and k_2 with observational datasets in section-III. We will evaluate the parameters γ_0 and k from the expression $\gamma_0 = \frac{H_0(n+3)}{1-k_2}$, and $k = \frac{3k_2}{(n+3)b_2} - 2$ for appropriate choice of arbitrary integrating constant b_2 and observationally constrained values of H_0, n and k_2.

KHDE: A generalized single-parameter entropy, known as the Kaniadakis entropy (κ-entropy) [77, 78, 79], is defined as

$$S_\kappa = -\sum_{i=1}^{W} \frac{P_i^{1+\kappa} - P_i^{1-\kappa}}{2\kappa} = \frac{1}{2}\left[\frac{\sum_{i=1}^{W}(P_i^{1-\kappa} - P_i)}{\kappa} + \frac{\sum_{i=1}^{W}(P_i^{1+\kappa} - P_i)}{-\kappa}\right], \tag{22}$$

where P_i denotes the probability of occupation of the i^{th} microstate of a classical system. The parameter κ encodes deviations from extensivity, and in the limit $\kappa \to 0$, the standard Boltzmann–Gibbs entropy is recovered [77, 78]. For an equiprobable distribution $P_i = 1/W$, Eq. (22) yields [77, 78, 79]

$$S_\kappa = \frac{W^\kappa - W^{-\kappa}}{2\kappa} \quad \Longrightarrow \quad S_\kappa = \frac{1}{\kappa}\sinh(\kappa S_{\text{BH}}), \tag{23}$$

where $S_{\text{BH}} \propto \dfrac{\mathcal{A}}{4G} = \dfrac{\pi L^2}{G}$ is the Bekenstein–Hawking entropy and G denotes Newton's constant.

Recently, Nojiri et al. [22, 23, 24] introduced a generalized four-parameter entropy function capable of reproducing several important entropy formalisms—such as Tsallis, Rényi, Barrow, Sharma–Mittal, Kaniadakis, and loop quantum gravity entropies—as special limiting cases. The proposed generalized entropy S_g is given by

$$S_g[\alpha_+, \alpha_-, \beta, \gamma] = \frac{1}{\gamma}\left[\left(1 + \frac{\alpha_+}{\beta}S_{\text{BH}}\right)^{\beta} - \left(1 + \frac{\alpha_-}{\beta}S_{\text{BH}}\right)^{-\beta}\right], \tag{24}$$

where $\alpha_+, \alpha_-, \beta$, and γ are positive parameters. For the particular limit $\beta \to \infty$ and $\alpha_+ = \alpha_- = \gamma/2 = \kappa$, Eq. (24) reduces to

$$S_\kappa = \frac{1}{\kappa}\sinh(\kappa S_{\text{BH}}), \tag{25}$$

which matches the Kaniadakis entropy in Eq. (23). Using the holographic principle, the energy density associated with the Kaniadakis entropy (23) takes the form

$$\rho_{de} \propto \frac{S_\kappa}{L^4} \quad \Longrightarrow \quad \rho_{de} = \frac{3c^2 M_p^2}{\kappa L^4}\sinh\left(\frac{\kappa\pi L^2}{G}\right), \tag{26}$$

where $M_p^2 = 1/(8\pi G)$ is the reduced Planck mass, L is the IR cutoff length scale, c is a model constant, and κ is the Kaniadakis parameter. In the Brans–Dicke (BD) framework, the gravitational coupling is dynamical, with $G = 1/\phi$. Substituting this relation into Eq. (26), the Kaniadakis holographic dark energy (KHDE) density becomes

$$\rho_{de} = \frac{3c^2\phi}{8\pi\kappa L^4}\sinh\left(\kappa\pi L^2\phi\right). \tag{27}$$

In holographic dark energy (HDE) models, the choice of the infrared (IR) cutoff is crucial for determining the cosmic dynamics. Among various possibilities, the Hubble horizon $\mathcal{L} = H^{-1}$ is considered one of the most natural and physically motivated options. The IR cutoff sets the largest length scale that contributes to the dark energy density. Different cutoffs, such as the particle or event horizons, can significantly alter the Universe's evolution. Unlike the event horizon, which depends on the future expansion history, the Hubble horizon is locally defined and free from causality issues. Therefore, adopting the Hubble radius as the IR cutoff provides a local, causal, and observationally consistent description of dark energy. By setting $\mathcal{L} = 1/H$, we obtain

$$\rho_{de} = \frac{3c^2 H^4\phi}{8\pi\kappa}\sinh\left(\frac{\kappa\pi\phi}{H^2}\right) \tag{28}$$

where Hubble parameter H is given by Eq. (20). Using Hubble parameter (20) in Eq. (28), we obtain the energy density of BHDE with Hubble horizon as IR cutoff as

$$\rho_{de} = \frac{3c^2 {k_1}^4 \left(\mathrm{e}^{\gamma_0 t}\right)^4 {\gamma_0}^4 \phi_0 \left(k_1 \mathrm{e}^{\gamma_0 t} + k_2\right)^{\frac{n}{n+3}-4}}{8\,(n+3)^4\,\pi\,\kappa} \sinh\left(\frac{\pi\,\kappa\,\phi_0\,(n+3)^2\left(k_1 \mathrm{e}^{\gamma_0 t} + k_2\right)^{\frac{3n+6}{n+3}}}{{k_1}^2\left(\mathrm{e}^{\gamma_0 t}\right)^2 {\gamma_0}^2}\right). \tag{29}$$

The BT-III universe with KHDE inside the framework of BDR theory of gravity is shown by Eq. (18), the scalar field (19), and the energy density (29). Using Eqs. (11), (12), (17), (19) and (29), we obtain the EoS parameter of our model as

$$\begin{aligned}
\omega_{de} \;=\; & \frac{8}{3}\frac{(n+3)^4\left(k_1 e^{\gamma_0 t}+k_2\right)^4 \pi\kappa}{c^2 k_1^4 e^{4\gamma_0 t}\gamma_0^4\phi_0}\left[\frac{1}{8}\frac{\phi_0(1-3\lambda)}{\pi(2-4\lambda)}\left(k_1 e^{\gamma_0 t}+k_2\right)^{\frac{n}{n+3}}\right. \\
& \times\left\{\frac{b_2^2 k_1^2\gamma_0^2 e^{2\gamma_0 t}+b_2 k_1 k_2^2\gamma_0^2 e^{\gamma_0 t}}{k_2^2(k_1 e^{\gamma_0 t}+k_2)^2}+\frac{k^2 b_2^2 k_1^2\gamma_0^2 e^{2\gamma_0 t}+k b_2 k_1 k_2^2\gamma_0^2 e^{\gamma_0 t}}{k_2^2(k_1 e^{\gamma_0 t}+k_2)^2}\right. \\
& \left.\left.+\frac{k b_2^2 k_1^2\gamma_0^2 e^{2\gamma_0 t}}{k_2^2(k_1 e^{\gamma_0 t}+k_2)^2}\right\}-\frac{1-\lambda}{2-4\lambda}\left(\frac{(k-1)\gamma_0^2 b_2 k_1 e^{\gamma_0 t}}{k_2(k_1 e^{\gamma_0 t}+k_2)}+\left(k_1 e^{\gamma_0 t}+k_2\right)^{-2b_2/k_2}\right)\right. \\
& -\frac{w\lambda n^2 k_1^2\gamma_0^2 e^{2\gamma_0 t}}{(2-4\lambda)(n+3)^2(k_1 e^{\gamma_0 t}+k_2)^2}-\frac{(2-\lambda)b_2 k_1^2\gamma_0^2 e^{2\gamma_0 t} n}{(1-2\lambda)k_2(k_1 e^{\gamma_0 t}+k_2)^2(n+3)} \\
& \left.-\frac{(\lambda+1)k b_2 k_1^2\gamma_0^2 e^{2\gamma_0 t} n}{(2-4\lambda)k_2(k_1 e^{\gamma_0 t}+k_2)^2(n+3)}-\frac{(\lambda+1)\left[n^2 k_1^2\gamma_0^2 e^{2\gamma_0 t}+n(n+3)k_1 k_2\gamma_0^2 e^{\gamma_0 t}\right]}{(2-4\lambda)(n+3)^2(k_1 e^{\gamma_0 t}+k_2)^2}\right] \\
& \times\left[\frac{(\lambda+1)(1-3\lambda)}{(2-4\lambda)^2}-\frac{(\lambda-1)(3-3\lambda)}{(2-4\lambda)^2}\right]^{-1}\left(k_1 e^{\gamma_0 t}+k_2\right)^{-\frac{n}{n+3}} \\
& \times\left[\sinh\left(\frac{\pi\kappa\phi_0(n+3)^2(k_1 e^{\gamma_0 t}+k_2)^2}{k_1^2 e^{2\gamma_0 t}\gamma_0^2}\left(k_1 e^{\gamma_0 t}+k_2\right)^{\frac{n}{n+3}}\right)\right]^{-1}.
\end{aligned} \tag{30}$$

and we find the skewness parameter as

$$\begin{aligned}
\gamma \;=\; & \frac{(n+3)^4\left(k_1\mathrm{e}^{\gamma_0 t}+k_2\right)^4\kappa}{3c^2{k_1}^4\left(\mathrm{e}^{\gamma_0 t}\right)^4{\gamma_0}^4}\left(\frac{(k-1)\,{\gamma_0}^2 b_2 k_1\mathrm{e}^{\gamma_0 t}}{k_2\left(k_1\mathrm{e}^{\gamma_0 t}+k_2\right)}+\left(\left(k_1\mathrm{e}^{\gamma_0 t}+k_2\right)^{\frac{b_2}{k_2}}\right)^{-2}\right) \\
& \times\left(\sinh\left(\frac{\pi\,\kappa\,\phi_0\,(n+3)^2\left(k_1\mathrm{e}^{\gamma_0 t}+k_2\right)^2}{{k_1}^2\left(\mathrm{e}^{\gamma_0 t}\right)^2{\gamma_0}^2}\left(k_1\mathrm{e}^{\gamma_0 t}+k_2\right)^{\frac{n}{n+3}}\right)\right)^{-1}.
\end{aligned} \tag{31}$$

3. OBSERVATIONAL CONSTRAINTS

The Hubble tension refers to the persistent discrepancy between independent determinations of the present-day expansion rate of the Universe, H_0, obtained from early- and late-time observations. Measurements inferred from the cosmic microwave background (CMB), particularly those based on Planck data within the ΛCDM framework, yield a lower value of $H_0 \approx 67$–$68\,\mathrm{km\,s^{-1}\,Mpc^{-1}}$, whereas direct local measurements using the cosmic distance ladder (Cepheids and Type Ia supernovae) favor a higher value of $H_0 \approx 73$–$74\,\mathrm{km\,s^{-1}\,Mpc^{-1}}$ [80, 81, 82, 83]. This discrepancy has now reached a statistical significance of $\sim 5\sigma$ or higher, and in some recent analyses even exceeds 6σ, indicating that it is unlikely to arise from statistical fluctuations alone [84, 85]. Independent observations, including those from the James Webb Space Telescope, continue to support the higher local value, reinforcing the robustness of the tension [86]. At present, no single systematic uncertainty has been identified that can fully account for this disagreement, suggesting that the tension may point toward new physics beyond the standard cosmological model. Proposed resolutions include early-Universe modifications such as early dark energy or additional relativistic species, as well as late-time extensions involving dynamical dark energy, interacting dark sectors, or modified theories of gravity. Consequently, the Hubble tension has emerged as one of the most significant challenges to ΛCDM and provides a powerful probe for testing extensions of the standard cosmological paradigm. The exact solutions of the field equations in Brans–Dicke–Rastall (BDR) gravity with anisotropic dark energy contain three free model parameters, namely (n, H_0, k_2), which explicitly appear in the expression for the Hubble parameter. The primary objective is to constrain these parameters using observational Hubble datasets in order to validate the model in the context of the present Universe. For this purpose, we employed a joint dataset consisting of 57 Hubble parameter measurements obtained from cosmic chronometer (CC) and baryon acoustic oscillation (BAO) observations [87, 88]. The numerical analysis was carried out using the `emcee` Python package, where the parameter space around the local minima was explored through a Gaussian prior centered on the initial estimates with a fixed standard deviation ($\sigma = 1.0$). The chi–square function used for parameter estimation is defined as

$$\chi^2_H(n, H_0, k_2) = \sum_{i=1}^{57} \frac{\left[H_{\mathrm{th}}(z_i; n, H_0, k_2) - H_{\mathrm{obs}}(z_i)\right]^2}{\sigma^2_{H(z_i)}}, \tag{35}$$

where $H_{\rm obs}(z_i)$ denotes the observed Hubble parameter at redshift z_i, $H_{\rm th}(z_i; n, H_0, k_2)$ represents the theoretically predicted value from the model, and $\sigma_{H(z_i)}$ corresponds to the associated observational uncertainty. By minimizing the above chi–square function and performing a Markov Chain Monte Carlo (MCMC) analysis, we obtained the best–fit estimates for the parameters n, H_0, and k_2 using the combined observational datasets.

Datasets	Parameter	Prior	Value
Hubble (CC+BAO Data)	H_0	$(50, 100)$	$67.90^{+0.28}_{-0.89}$
	k_2	$(-1, 0)$	$-0.448^{+0.077}_{-0.068}$
	n	$(-2, -1)$	$-1.215^{+0.079}_{-0.092}$
	b_2	–	-0.26
	k	–	$+0.91^{+0.5265}_{-0.1840}$
	b_1	–	0.3

Table 1. The MCMC estimates.

Fig. 1 presents the marginalized one–dimensional posterior distributions and the two–dimensional confidence contours for the model parameters (k_2, H_0, n) obtained from the joint CC+BAO dataset using the Markov Chain Monte Carlo (MCMC) technique. The MCMC analysis efficiently explores the parameter space and provides robust constraints by minimizing the corresponding χ^2 function. From the one–dimensional posteriors, we obtain the best–fit values $k_2 = -0.448^{+0.077}_{-0.068}$, $H_0 = 67.90^{+0.28}_{-0.89}$, and $n = -1.215^{+0.079}_{-0.092}$ at the 1σ confidence level. The inferred value of the Hubble parameter H_0 is in good agreement with recent observational estimates, indicating the consistency of the present model with late–time cosmic expansion data. The two–dimensional contour plots show well–defined closed regions at 1σ and 2σ confidence levels, implying a strong correlation among the parameters and the statistical stability of the model. Fig. 2 shows the comparison between the reconstructed Hubble parameter $H(z)$ obtained from the best–fit model parameters and the observational CC+BAO data. The solid curve represents the best–fit evolution of $H(z)$, while the shaded regions correspond to the 1σ and 2σ confidence intervals derived from the MCMC analysis. The observational data points are found to lie well within the confidence regions across the entire redshift range, indicating an excellent agreement between the theoretical model and observations. For comparison, the standard ΛCDM prediction is also shown and exhibits a slightly different evolution at intermediate and higher redshifts. The close proximity of the best–fit curve to the ΛCDM model at low redshifts confirms that the present model successfully reproduces the observed late–time cosmic expansion. At higher redshifts, small deviations appear, reflecting the influence of anisotropy and modified gravity effects inherent in the model. Overall, the consistency of the reconstructed $H(z)$ with CC+BAO data demonstrates the robustness and observational viability of the proposed cosmological framework.

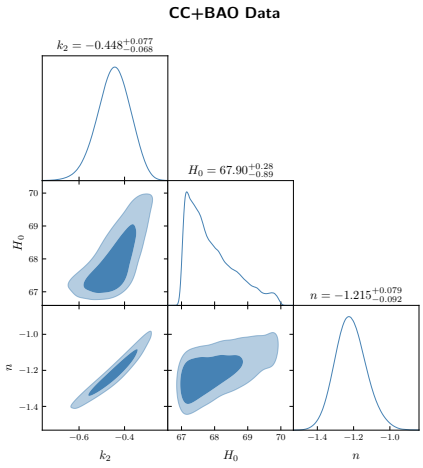

Figure 1. The 2D contour plots of H_0, n, k_2 at $\sigma 1$ and $\sigma 2$ level of confidence in the joint MCMC analysis of CC+BAO datasets.

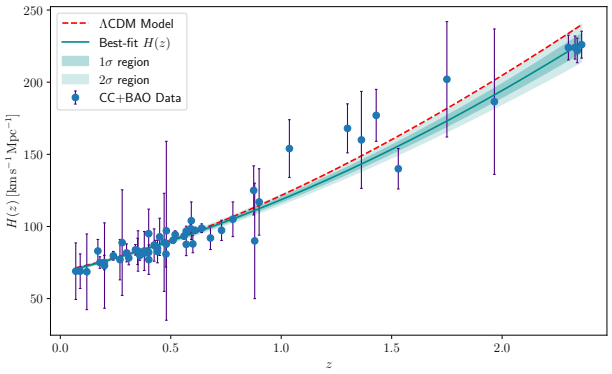

Figure 2. Evolution of Hubble parameter $H(z)$ versus redshift z. The solid line represents our model and dotted-line indicates the ΛCDM model with $\Omega_{m0} = 0.3$ and $\Omega_{\Lambda 0} = 0.7$. The dots are shown the Hubble dataset with error bar.

4. COSMOLOGICAL PARAMETERS

In this section, we examine the expansion dynamics of the Universe within the constructed KHDE model by employing several standard cosmological diagnostics. These include the equation of state (EoS) parameter ω_{de}, the squared

sound speed v_s^2, the deceleration parameter q, and the Om–diagnostic $Om(z)$. Furthermore, we analyze the evolutionary behavior of the model through well–known diagnostic planes such as the ω_{de}–ω'_{de} plane, the statefinder pair (r, s), and the r–q plane. For the graphical and numerical analysis, we adopt the constrained parameter values $H_0 = 67.9$, $k_2 = -0.448$, and $n = -1.215$, obtained from observational datasets. In addition, the derived and auxiliary parameters are chosen as $\gamma_0 = 83.7$, $k = 0.91$, $b_1 = 0.3$, $b_2 = -0.26$, $c = 0.03$, $\lambda = 0.7$, $\phi_0 = 95$, $\omega = 0.6$, and $\kappa = 0.2$. These parameter choices ensure physically consistent behavior of the cosmological quantities and provide a representative visualization of the model's dynamical evolution.

Scalar field

Fig. 3 illustrates the evolution of the scalar field ϕ as a function of redshift z. It is observed that the scalar field exhibits a monotonically increasing behaviour with increasing redshift, indicating that ϕ attains smaller values at late times and grows significantly toward the early universe. This behaviour suggests that the effective gravitational coupling, which is inversely related to the scalar field in Brans–Dicke theory, was stronger in the past and gradually weakens as the universe expands. Such an evolution is physically reasonable and consistent with scalar–tensor cosmological models, where deviations from general relativity are more prominent at early epochs. Moreover, the gradual growth of the scalar field supports a stable cosmic evolution and ensures compatibility with current observational constraints. Hence, the obtained scalar field dynamics reinforces the viability of the present cosmological model.

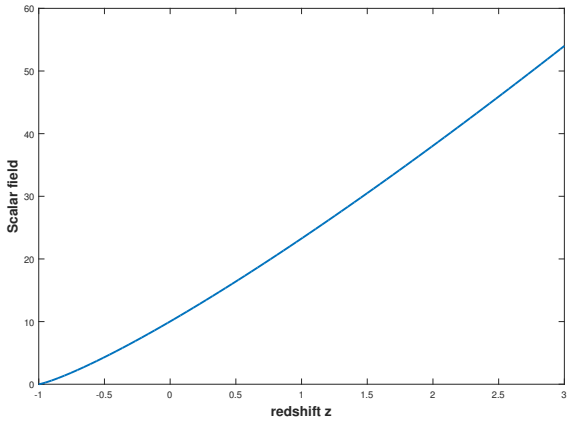

Figure 3. The plot between scalar field $\phi(z)$ and redshift z.

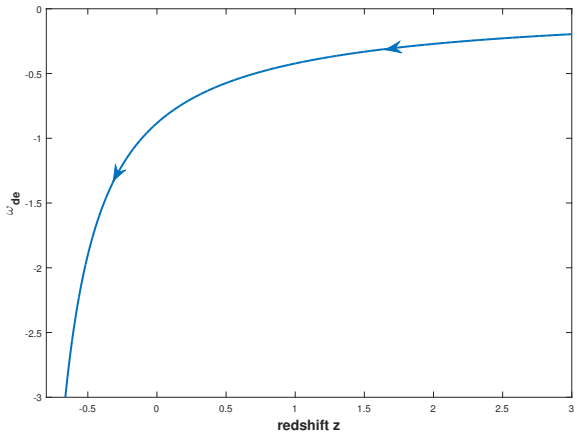

Figure 4. Plot of EoS parameter versus redshift z.

EoS parameter

The equation of state (EoS) parameter $\omega_{de} = p_{de}/\rho_{de}$ plays a fundamental role in understanding the dynamical nature of dark energy and the expansion history of the universe. Different values of ω_{de} correspond to distinct evolutionary phases, ranging from early decelerating epochs to the present accelerated expansion. Fig. 4 illustrates the evolution of the dark energy EoS parameter as a function of redshift z for the present model. From the Fig. 4, it is evident that ω_{de} remains less than -1 over a significant redshift range, indicating a phantom–like behaviour of dark energy. Such a regime is capable of driving strong accelerated expansion and is consistent with recent observational indications that mildly favor phantom or dynamical dark energy over a strict cosmological constant. At higher redshifts, the EoS parameter gradually approaches values closer to $\omega_{de} \to -1$, suggesting that the model effectively mimics a ΛCDM–like behaviour. The continuous transition of the EoS parameter reflects the dynamical nature of dark energy in the model, rather than a constant vacuum energy density. Overall, the evolution of the EoS parameter demonstrates that the proposed model successfully accounts for the present accelerated expansion of the universe while remaining consistent with a smooth cosmic evolution.

Deceleration parameter

The deceleration parameter $q(z)$ plays a crucial role in characterizing the expansion history of the universe, as its sign directly distinguishes between decelerated and accelerated phases of cosmic evolution. Physically, q measures the rate of change of the cosmic expansion relative to the Hubble expansion rate. If $q > 0$, the universe is in a decelerated expansion phase, while $q < 0$ indicates accelerated expansion. The case $q = 0$ corresponds to uniform expansion. The

redshift evolution of $q(z)$ allows us to determine the transition redshift at which the universe shifted from matter-dominated deceleration to dark-energy-driven acceleration. For our models it is defined as

$$q = -\frac{\ddot{a}a}{\dot{a}^2} = -1 - \frac{k_2\,(n+3)}{k_1 e^{\gamma_0 t}}. \tag{32}$$

where $a(t)$ is the scale factor. Fig. 5 depicts the evolution of q as a function of redshift z for the present model constrained by the CC+BAO data. At early times (higher redshifts), the deceleration parameter remains positive ($q > 0$), indicating a decelerating expansion phase dominated by matter and anisotropic effects. This behaviour is consistent with the standard cosmological picture of a matter-dominated universe in the past. As the universe evolves, $q(z)$ decreases monotonically and crosses the phantom divide line $q = 0$ at the transition redshift $z_t \simeq 0.79$, signaling a smooth transition from decelerated to accelerated expansion. Such a transition redshift is well supported by recent observational studies, thereby reinforcing the observational consistency of the model. At the present epoch ($z = 0$), the deceleration parameter attains a negative value $q_0 \approx -0.45$, confirming that the universe is currently undergoing accelerated expansion. Overall, the evolution of the deceleration parameter demonstrates that the model successfully describes a realistic and smooth cosmic expansion history.

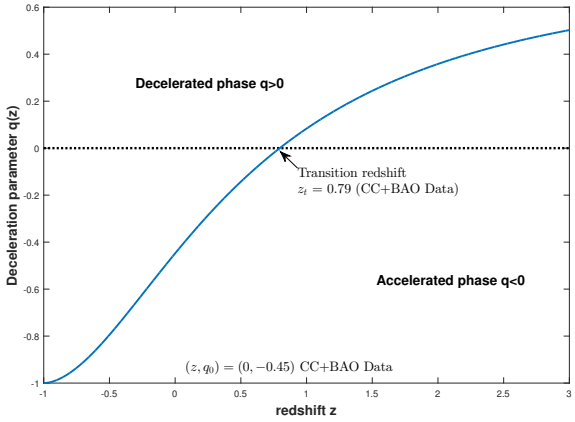

Figure 5. The plot between deceleration parameter q versus redshift z.

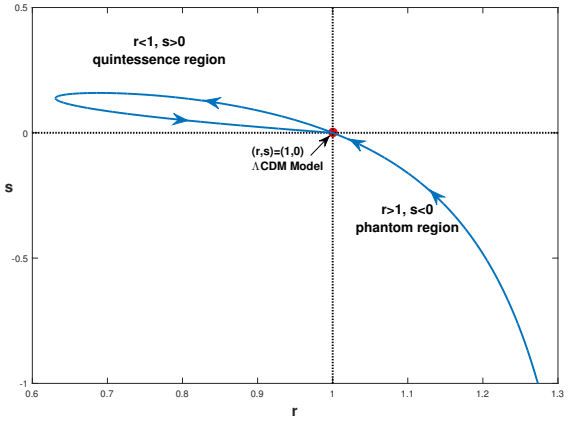

Figure 6. The plot of statefinder parameters.

Satefinders plane

In order to discriminate among various DE models that successfully explain the late–time accelerated expansion of the universe, higher–order geometrical diagnostics are required. Although different DE models can reproduce the same present–day values of the Hubble parameter H and the deceleration parameter q, these quantities alone are insufficient to distinguish between competing scenarios. To overcome this limitation, Sahni et al. [89] introduced the statefinder diagnostic pair (r, s), defined in Eq. (33), which depends on the third derivative of the scale factor and hence captures finer details of cosmic dynamics. Fig. 6 displays the evolution of the present model in the (r, s) plane. The trajectory clearly passes through different DE regimes, thereby offering a clear geometrical interpretation of the cosmic evolution. At early times, the trajectory lies in the region characterized by $r > 1$ and $s < 0$, which corresponds to the phantom–like dark energy regime. This behaviour indicates a strong acceleration phase driven by effective DE with an equation of state less than -1. As the universe evolves, the trajectory approaches the fixed point $(r, s) = (1, 0)$, which represents the standard ΛCDM model. The proximity of the trajectory to this point at late times implies that the present model closely mimics the concordance cosmology and is therefore consistent with current observations. At later epochs, the evolution enters the region $r < 1$ and $s > 0$, which is associated with quintessence–type DE behaviour. This transition signifies a gradual softening of the acceleration mechanism and reflects the dynamical nature of DE in the present framework. Overall, the statefinder analysis demonstrates that the proposed cosmological model is capable of interpolating between different DE regimes while remaining compatible with the ΛCDM limit.

$$r = 1 + \frac{3k_2\,(n+3)}{k_1 e^{\gamma_0 t}} + \frac{{k_2}^2\,(n+3)^2}{{k_1}^2\,(e^{\gamma_0 t})^2} - \frac{k_2\,(n+3)^2}{k_1 e^{\gamma_0 t}}$$

$$s = \left(\frac{3k_2\,(n+3)}{k_1 e^{\gamma_0 t}} + \frac{{k_2}^2\,(n+3)^2}{{k_1}^2\,(e^{\gamma_0 t})^2} - \frac{k_2\,(n+3)^2}{k_1 e^{\gamma_0 t}}\right)\left(-4.5 - \frac{3k_2\,(n+3)}{k_1 e^{\gamma_0 t}}\right)^{-1} \tag{33}$$

$r - q$ plane

The r–q plane provides a useful geometrical diagnostic to study the evolutionary behavior of cosmological models and to distinguish them from standard dark energy scenarios. In this plane, the fixed point $(r, q) = (1, 0.5)$ corresponds to the standard cold dark matter (SCDM) dominated universe, while the point $(r, q) = (1, -1)$ represents the steady state (SS) or de Sitter model, characterized by a constant expansion rate and exponential growth of the scale factor. The evolution of the present model in the r–q plane is shown in Fig. 7. From the Fig. 7, it is evident that the trajectory of the model begins in the vicinity of the SCDM point at early times, indicating that the universe undergoes a decelerated expansion phase dominated by matter. As cosmic time progresses, the trajectory smoothly departs from the SCDM fixed point and moves toward negative values of the deceleration parameter, reflecting the onset of late–time accelerated expansion. This transition signifies the gradual dominance of dark energy–like effects over matter. At late times, the trajectory approaches the steady state point $(r, q) = (1, -1)$, which corresponds to a de Sitter–type expansion. This behavior suggests that the universe evolves toward a phase of exponential expansion driven by an effective cosmological constant. The smooth and continuous nature of the trajectory confirms the absence of abrupt transitions or singular behavior, ensuring the physical stability of the model. Furthermore, the evolutionary path of the model closely resembles the expected behavior of the ΛCDM scenario, which evolves from the SCDM regime toward the steady state limit.

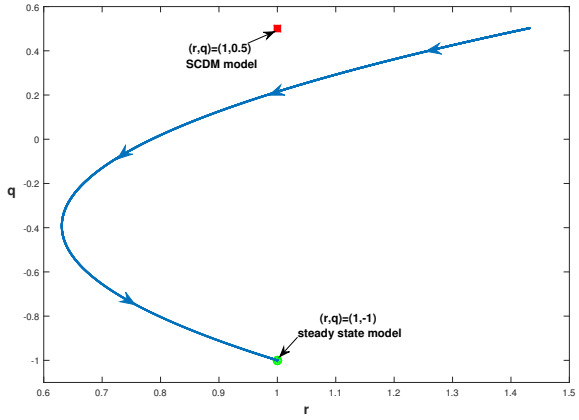

Figure 7. The plot of $Om(z)$ versus z.

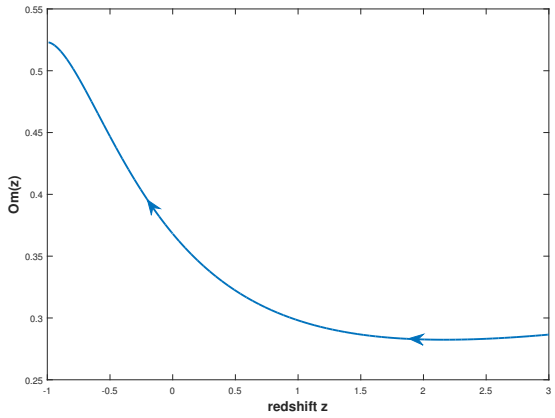

Figure 8. The plot between ω_{de} versus its derivative ω'_{de}.

Om-diagnostic parameter

The $Om(z)$ diagnostic provides an effective and model–independent tool to characterize the nature of dark energy by directly relating the Hubble parameter $H(z)$ to the redshift z. Unlike the equation of state parameter, the $Om(z)$ diagnostic does not require higher–order derivatives of the scale factor, making it particularly robust against observational uncertainties. In the standard ΛCDM cosmology, $Om(z)$ remains constant and positive for all redshifts, reflecting a constant dark energy density associated with a cosmological constant. It is defined as

$$Om(z) = \frac{H^2(z) - H_0^2}{((z+1)^3 - 1)H_0^2} = \frac{\left[\frac{1-k_2(1+z)^{n+3}}{1-k_2}\right]^2 - 1}{(z+1)^3 - 1}. \tag{34}$$

Fig. 8 illustrates the evolution of $Om(z)$ for the present model. It is evident that $Om(z)$ exhibits a clear decreasing trend with increasing redshift over a wide redshift range. Such a monotonic decrease in $Om(z)$ is a characteristic signature of phantom–like dark energy. This behaviour implies that the dark energy density grows with cosmic time, leading to a stronger acceleration at late epochs. The deviation of $Om(z)$ from a constant value further confirms that the present model does not reduce exactly to the ΛCDM scenario but represents a dynamically evolving dark energy framework. At higher redshifts, $Om(z)$ approaches a nearly constant value, indicating that the influence of dark energy becomes subdominant and the cosmic expansion is primarily governed by matter. This feature is consistent with the expected transition from a matter–dominated decelerating phase in the past to a dark energy–dominated accelerated phase at late times. Hence, the $Om(z)$ diagnostic strongly supports the viability of the proposed model as a realistic and physically consistent description of dark energy.

$\omega_{de} - \omega'_{de}$ Plane

The ω_{de}–ω'_{de} phase–space analysis serves as an important diagnostic tool to investigate the dynamical nature of dark energy, where the prime denotes differentiation with respect to $\ln a$. This method, introduced by Caldwell and Linder [90],

enables a clear classification of dark energy models based on their evolutionary behavior. In this framework, dark energy models are broadly categorized into two distinct regions: the thawing region, characterized by $\omega_{de} < 0$ and $\omega'_{de} > 0$, and the freezing region, where $\omega_{de} < 0$ and $\omega'_{de} < 0$. Fig. 9 depicts the evolution of the present model in the ω_{de}–ω'_{de} plane. It is evident that the trajectory lies entirely in the region $\omega_{de} < 0$ with $\omega'_{de} < 0$, which clearly corresponds to the freezing class of dark energy models. This behavior indicates that the dark energy equation of state evolves toward $\omega_{de} = -1$ at late times, gradually slowing down its dynamical evolution and mimicking a cosmological constant–like behavior in the future. The freezing nature of the model suggests that dark energy was more dynamic in the past and becomes increasingly dominant and stable as the universe expands. The ω_{de}–ω'_{de} analysis strongly supports that the present model belongs to the freezing dark energy class and provides a viable dynamical alternative to the standard ΛCDM model while remaining consistent with current observational constraints.

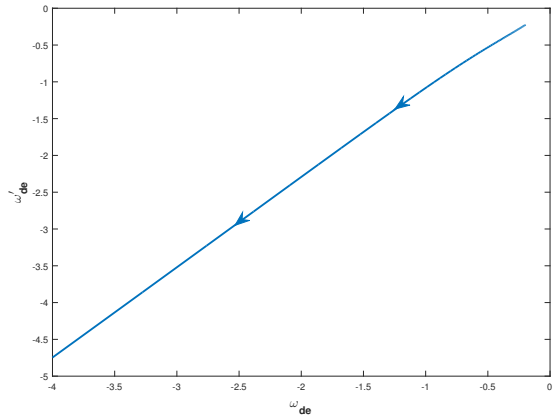

Figure 9. The plot between ω_{de} versus its derivative ω'_{de}.

Age of the model

The cosmic time $t(z)$ and the lookback time $t_0 - t(z)$ are important quantities for understanding the age and evolutionary history of the universe. We estimate the age of our model using:

$$t_0 - t = \int_0^z \frac{dz'}{(1+z')H(z')}. \tag{35}$$

For our model, we have obtained the expression for cosmic age of the universe as

$$t_0 - t = \frac{k_2 - 1}{(n+3)H_0} \ln\left[\frac{1 - k_2(1+z)^{n+3}}{(1-k_2)(1+z)^{n+3}}\right]. \tag{36}$$

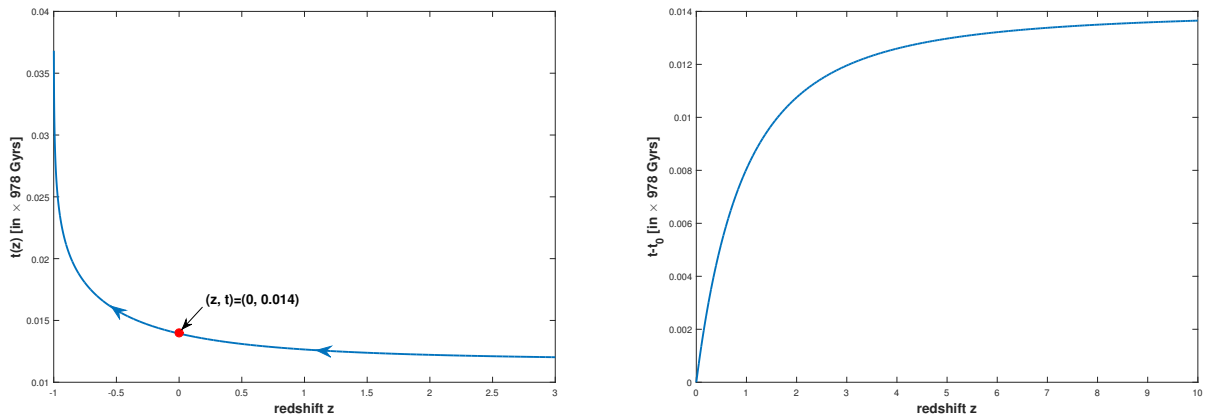

(a) (b)

Figure 10. The plot between cosmic time difference $t_0 - t$ and $t(z)$ versus redshift z.

Fig. 10(a) shows the variation of the cosmic time t as a function of redshift z. At the present epoch ($z = 0$), the cosmic time attains the value $t_0 \simeq 0.014 \times 978$ Gyr = 13.78 Gyr, which represents the current age of the universe in the adopted units. As z increases, $t(z)$ decreases rapidly, reflecting the faster expansion rate in the early universe. Fig. 10(b) illustrates the behaviour of the lookback time $t_0 - t(z)$ as a function of redshift. The lookback time increases monotonically with redshift, indicating that light emitted from higher redshifts has traveled longer durations before reaching the observer. At low redshifts, $t_0 - t(z)$ grows rapidly, while at higher redshifts the curve gradually flattens, showing that most of the cosmic age is accumulated at relatively small redshifts. This behaviour is consistent with an early decelerated expansion followed by a late-time accelerated phase. The smooth and regular evolution of both $t(z)$ and $t_0 - t(z)$ confirms the absence of any sudden transitions or singular behaviour in the cosmic history. Moreover, the consistency between the decreasing cosmic time and increasing lookback time reinforces the physical reliability of the present cosmological model and supports its compatibility with the standard picture of cosmic evolution.

5. CONCLUSIONS

In this work, we have investigated an anisotropic Bianchi type–III cosmological model filled with KHDE and pressureless matter within the framework of BDR theory of gravity. The combination of anisotropic geometry, modified gravity, and generalized holographic dark energy provides a rich and flexible framework to study cosmic evolution. By imposing suitable relations among the metric potentials and assuming a functional dependence between the Brans–Dicke scalar field and the average scale factor, we obtained exact analytical solutions of the field equations. Using these solutions, several key cosmological parameters were derived and analyzed in detail. The evolution of the Hubble parameter shows a smooth and physically reasonable behavior, consistent with observational data. In particular, the reconstructed $H(z)$ profile obtained from the best–fit parameters lies well within the 1σ and 2σ confidence regions of the CC+BAO datasets, demonstrating the robustness of the model against current observations. The model parameters were tightly constrained using a MCMC analysis with CC+BAO datasets. The resulting best–fit values, particularly for the Hubble constant, are in good agreement with recent observational estimates. The well–defined and closed confidence contours in the parameter space confirm the statistical stability and convergence of the MCMC analysis.

The deceleration parameter analysis reveals a clear transition from an early decelerated phase to the present accelerated phase of the universe. The transition redshift obtained in this model is compatible with recent observational constraints, confirming that the model can successfully reproduce the observed cosmic acceleration. This smooth transition further supports the physical viability of the model. The behavior of the equation of state parameter of dark energy plays a crucial role in characterizing the nature of cosmic acceleration. Our analysis shows that the EoS parameter remains in the phantom region throughout the evolution, implying $\omega_{de} < -1$. Such a behavior is capable of driving strong accelerated expansion and is consistent with several recent observational indications favoring dynamical dark energy over a strict cosmological constant. Importantly, the evolution of ω_{de} is smooth and free from divergences, indicating the absence of pathological future singularities within the considered redshift range. To further discriminate the present model from standard dark energy scenarios, we employed several geometrical diagnostics, including the statefinder (r, s) and (r, q) planes, as well as the $Om(z)$ diagnostic. The statefinder analysis shows that the evolutionary trajectory of the model passes through different dark energy regimes and approaches the ΛCDM fixed point at late times, indicating that the model can effectively mimic the concordance cosmology in the recent past while allowing deviations at earlier epochs. Similarly, the r–q plane demonstrates a smooth evolution from the standard cold dark matter dominated era toward a de Sitter–like steady state, reinforcing the consistency of the model with the expected cosmic history. The $Om(z)$ diagnostic exhibits a decreasing trend with redshift, which further confirms the phantom–like nature of dark energy in this framework and rules out a constant ΛCDM behavior. We also analyzed the evolution of the Brans–Dicke scalar field and the cosmic time parameters. The scalar field shows a regular and monotonic behavior, suggesting a time–varying effective gravitational coupling that evolves smoothly with cosmic expansion. The cosmic time and lookback time analyses indicate a consistent and realistic age of the universe, with no abrupt transitions or singular behavior, thereby strengthening the physical reliability of the model.

In conclusion, the present study demonstrates that the KHDE model within the BDR framework provides a viable and observationally consistent description of the cosmic expansion history in an anisotropic universe. The model successfully explains the transition from early deceleration to late–time acceleration, closely mimics ΛCDM behavior at late times, and allows for a dynamical dark energy component with phantom characteristics. These results highlight the potential of generalized holographic dark energy models in modified gravity theories as promising alternatives to the standard cosmological paradigm.

Acknowledgment

We sincerely thank the reviewer for their constructive and insightful comments, which have helped to substantially improve the presentation of this work. The work has been supported financially by National Board for Higher Mathematics, Department of Atomic Energy, Govt. of India under the Research project No.: 02011/8/2023 NBHM(R.P.)/R & D II/3073.

ORCID

Y. Aditya, https://orcid.org/0000-0002-5468-9697; **K. Dasunaidu**, https://orcid.org/0000-0003-3583-2432;
Muralasetti Nookaraju, https://orcid.org/0000-0002-3743-8036;
G. Suryanarayana, https://orcid.org/0000-0002-4866-4020

REFERENCES

[1] J. R. Primack, Nucl. Phys. B Proc. Suppl. **173**, 1 (2007). https://doi.org/10.1016/j.nuclphysbps.2007.08.152
[2] F. Zwicky, Helv. Phys. Acta, **6**, 110 (1933). https://doi.org/10.1007/s10714-008-0707-4
[3] S. Nojiri, and S. D. Odintsov, Phys. Lett. B, 639, 144 (2006). https://doi.org/10.1016/j.physletb.2006.06.065
[4] K. Bamba, *et al*., Astrophys. Space Sci. **342**, 155 (2012). https://doi.org/10.1007/s10509-012-1181-8
[5] E. J. Copeland, *et al*., Int. J. Mod. Phys. D, **15**, 1753 (2006). https://doi.org/10.1142/s021827180600942x
[6] S. Nojiri, and S. D. Odintsov, Phys. Rept. **505**, 59 (2011). https://doi.org/10.1016/j.physrep.2011.04.001
[7] S. Weinberg, *Gravitation and Cosmology*, (Wiley, New York, 1972).
[8] C. Brans, R.H., Dicke, Phys. Rev. **124**, 925 (1961). https://doi.org/10.1103/physrev.124.925
[9] N. Banerjee, and D. Pavon, Phys. Rev. D, **63**, 043504 (2001). https://doi.org/10.1103/physrevd.63.043504
[10] A. Khodam-Mohammadi, *et al*., Int. J. Mod. Phys. D, **23**, 1450081 (2014). https://doi.org/10.1142/S0218271814500813
[11] S. Kazempour, and A. R. Akbarieh, Phys. Rev. D, **105**, 123515 (2022). https://doi.org/10.1103/PhysRevD.105.123515
[12] A. G. Cohen, *et al*., Phys. Rev. Lett. **82**, 4971 (1999). https://doi.org/10.1103/physrevlett.82.4971
[13] P. Horava, and D. Minic, Phys. Rev. Lett. **85**, 1610 (2000). https://doi.org/10.1103/physrevlett.85.1610
[14] S. Wang, *et al*., Phys. Rept. **696**, 1 (2017). https://doi.org/10.1016/j.physrep.2017.06.003
[15] M. Jamil, *et al*., Int. J. Theor. Phys. **51**, 604 (2012). https://doi.org/10.1007/s10773-011-0940-6
[16] M. Tavayef, *et al*., Phys. Lett. B, **781**, 195 (2018). https://doi.org/10.1016/j.physletb.2018.04.001
[17] H. Moradpour, *et al*., Eur. Phys. J. C, **80**, 732 (2020). https://doi.org/10.1140/epjc/s10052-020-8307-x
[18] S. Nojiri, S. D. Odintsov, and V. Faraoni, Phys. Rev. D, **105**, 044042 (2022). https://doi.org/10.1103/physrevd.105.044042
[19] M. Tavayef, *et al*., Phys. Lett. B, **781**, 195 (2018). https://doi.org/10.1016/j.physletb.2018.04.001
[20] A.S. Jahromi, *et al*., Phys. Lett. B, **780**, 21 (2018). https://doi.org/10.1016/j.physletb.2018.02.052
[21] H. Moradpour, *et al*. Eur. Phys. J. C, **78**, 829 (2018). https://doi.org/10.1140/epjc/s10052-018-6309-8
[22] S. Nojiri, *et al*., Phys. Rev. D, **105**, 044042 (2022). https://doi.org/10.1103/PhysRevD.105.044042
[23] S. Nojiri, *et al*., Universe, **10**, 352 (2024). https://doi.org/10.3390/universe10090352
[24] S. Nojiri, *et al*., Phys. Lett. B, **831**, 137189 (2022). https://doi.org/10.1016/j.physletb.2022.137189
[25] G. Kaniadakis, Physica A: Stat. Mech. and its Appl. **296(3-4)**, 405 (2001). https://doi.org/10.1016/s0378-4371(01)00184-4
[26] M. Masi, Phys. Lett. A, **338**, 217 (2005). https://doi.org/10.1016/j.physleta.2005.01.094
[27] E. M. Abreu, *et al*., EPL (Europhysics Letters), **124**, 30003 (2018). https://doi.org/10.1209/0295-5075/124/30003
[28] H. Moradpour, *et al*. Eur. Phys. J. C, **80**, 1 (2020). https://doi.org/10.1140/epjc/s10052-020-8307-x
[29] P. Rastall, Phys. Rev. D, **6**, 3357 (1972). https://doi.org/10.1103/physrevd.6.3357
[30] N. D. Birrell, and P. C. W. Davies, *Quantum fields in curved space*, (Cambridge University Press, Cambridge, 1982).
[31] C. E. M. Batista, *et al*., Phys. Rev. D **85**, 084008 (2012). https://doi.org/10.1103/PhysRevD.85.084008
[32] W. A. G. De Moraes, and A. F. Santos, Gen. Relativ. Grav. **51**, 167 (2019). https://doi.org/10.1007/s10714-019-2652-9
[33] H. Shabani, and A. H. Ziaie, EPL **129**, 20004 (2020). https://doi.org/10.1209/0295-5075/129/20004
[34] F. Darabi, *et al*., Eur. Phys. J. C, **78**, 25 (2018). https://doi.org/10.1140/epjc/s10052-017-5502-5
[35] M. Visser, Phys. Lett. B, **782**, 83 (2018). https://doi.org/10.1016/j.physletb.2018.05.028
[36] A. Singh, G.P. Singh, and A. Pradhan, Int. J. Mod. Phys. A, **37**, 2250104 (2022). https://doi.org/10.1142/S0217751X22501044
[37] A. Singh, and A. Pradhan, Indian J. Phys. **97**, 631 (2023). https://doi.org/10.1007/s12648-022-02406-z
[38] J. W. Moffat, Phys. Lett. B, **355**, 447 (1995). https://doi.org/10.1016/0370-2693(95)00670-g
[39] J. D. Bekenstein, Phys. Rev. D, **70**, 083509 (2004). https://doi.org/10.1103/physrevd.70.083509
[40] H. Bondi, and T. Gold, Mon. Not. R. Astron. Soc. **108**, 252 (1948). https://doi.org/10.1093/mnras/108.3.252
[41] F. Hoyle, Mon. Not. R. Astron. Soc. **108**, 372 (1948). https://doi.org/10.1093/mnras/108.5.372
[42] M.V. Santhi, *et al*., Int. J. Geo. Meth. Mod. Phys. **15**, 1850161 (2018). https://doi.org/10.1142/s021988781850161x
[43] K. D. Raju, *et al*., Astrophys. Space Sci. **365**, 45 (2020). https://doi.org/10.1007/s10509-020-03753-1
[44] K.D. Naidu, *et al*., Mod. Phys. A, **36**, 2150054 (2021). https://doi.org/10.1142/S0217732321500541

[45] Y. Aditya, *et al.*, New Astr. **84**, 101504 (2021). https://doi.org/10.1016/j.newast.2020.101504
[46] M.P.V.V. Bhaskara Rao, *et al.*, Int. J. Mod. Phys. A, **36**, 2150260 (2021). https://doi.org/10.1142/S0217751X21502602
[47] Y. Aditya, *et al.*, Int. J. Mod. Phys. A, **37**, 2250107 (2022). https://doi.org/10.1142/S0217751X2250107X
[48] U.Y.D. Prasanthi, and Y. Aditya, Phys. Dark Univ. **31**, 100782 (2021). https://doi.org/10.1016/j.dark.2021.100782
[49] Y. Aditya, U.Y.D. Prasanthi, Bulg. Astr. Journal, **38**, 52 (2023). https://astro.bas.bg/AIJ/issues/n39/YAditya.pdf
[50] U.Y.D. Prasanthi, and Y. Aditya, Results Phys. **17**, 103101 (2020). https://doi.org/10.1016/j.rinp.2020.103101
[51] Y. Aditya, Bulg. Astr. Journal, **39**, 12 (2023). https://astro.bas.bg/AIJ/issues/n39/YAditya.pdf
[52] Y. Aditya, Bulg. Astr. Journal, **40**, 95 (2024). https://astro.bas.bg/AIJ/issues/n40/YAditya.pdf
[53] U.K. Sharma, *et al.*, IJMPD, **31(03)**, 2250013 (2022). https://doi.org/10.1142/S0218271822500134
[54] J. Sadeghi, et al., Mod. Phys. Lett. A, **38**, 2350076 (2023). https://doi.org/10.1142/S0217732323500761
[55] B.G. Rao, *et al.*, East Eur. J. Phys. (1), 43 (2024). https://doi.org/10.26565/2312-4334-2024-1-03
[56] A.V. Prasanthi, *et al.*, East Eur. J. Phys. (2), 10 (2024). https://doi.org/10.26565/2312-4334-2024-2-01
[57] S. Ghaffari, Mod. Phys. Lett. A, **37**, 2250152 (2022). https://doi.org/10.1142/S0217732322501528
[58] S. Ali, *et al.*, New Astr. **110**, 102226 (2024). https://doi.org/10.1016/j.newast.2024.102226
[59] K. Murali, *et al.*, Mod. Phys. Lett. A, **39**, 2450106 (2024). https://doi.org/10.1142/S0217732324501062
[60] K. Murali, *et al.*, AIP Conf. Proc. **3298**, 040022 (2025). https://doi.org/10.1063/5.0279370
[61] K.S. Thorne, Astrophys. J. **148**, 51 (1967). https://doi.org/10.1086/149127
[62] J. Kristian, and R.K. Sachs, Astrophys. J. **143**, 379 (1966). https://doi.org/10.1086/148522
[63] R. Kantowski, and R.K. Sachs, J. Math. Phys. **7**, 433 (1966). https://doi.org/10.1063/1.1704952
[64] C.B. Collins, *et al.*, Gen. Relativ. Gravit. **12**, 805 (1980). https://doi.org/10.1007/bf00763057
[65] V.B. Johri, and R. Sudharsan, Australian Journal of Physics, **42(2)**, 215 (1989). https://doi.org/10.1071/ph890215
[66] V.B. Johri, and K. Desikan, Gen. Relat. Gravit. **26**, 1217 (1994). https://doi.org/10.1007/bf02106714
[67] M.V. Santhi, *et al.*, Can. J. Phys., **94(6)**, 578 (2016). https://doi.org/10.1139/cjp-2016-0099
[68] Y. Aditya, *et al.*, Astrophys Space Sci. **364**, 190 (2019). https://doi.org/10.1007/s10509-019-3681-2
[69] Y. Aditya, *et al.*, Eur. Phys. J. C, **79**, 1020 (2019). https://doi.org/10.1140/epjc/s10052-019-7534-5
[70] Y. Aditya, and D.R.K. Reddy, Eur. Phys. J. C, **78**, 619 (2018). https://doi.org/10.1140/epjc/s10052-018-6074-8
[71] Ö. Akarsu, and C.B. Kilinc, Gen. Relativ. Gravit. **42**, 119 (2010). https://doi.org/10.1007/s10714-009-0821-y
[72] M. Sharif, and M. Zubair, Astrophys. Space Sci. **330**, 399 (2010). https://doi.org/10.1007/s10509-010-0414-y
[73] K.S. Adhav, Int. J. Astron. Astrophys. **1**, 204 (2011). https://doi.org/10.1007/s10509-011-0773-z
[74] M.V. Santhi, *et al.*, Astrophys. Space Sci. **361**, 142 (2016). https://doi.org/10.1007/s10509-016-2731-2
[75] M.V. Santhi, *et al.*, Can. J. Phys. **95**, 179 (2017). https://doi.org/10.1139/cjp-2016-0628
[76] Y. Aditya, and D.R.K. Reddy, Astrophys Space Sci. **363**, 207 (2018). https://doi.org/10.1007/s10509-018-3429-4
[77] G. Kaniadakis, Physica A: Statistical Mechanics and its Applications, **296**, 405 (2001). https://doi.org/10.1016/s0378-4371(01)00184-4
[78] G. Kaniadakis, Phys. Rev. E, **66**, 5 (2002). https://doi.org/10.1103/physreve.66.056125
[79] H. Moradpour, *et al.*, Eur. Phys. J. C, **80**, 8 (2020). https://doi.org/10.1140/epjc/s10052-020-8307-x
[80] N. Aghanim, *et al.*, A&A, **641**, A6 (2020). https://doi.org/10.1051/0004-6361/201833910
[81] A.G. Riess, *et al.*, Astrophys. J. Lett. **934**, L7 (2022). https://doi.org/10.3847/2041-8213/ac5c5b
[82] V. Poulin, *et al.*, Phys. Rev. D **111**, 083552 (2025). https://doi.org/10.1103/PhysRevD.111.083552
[83] B. Cousins, *et al.*, arXiv:2503.01997 (2026). https://doi.org/10.48550/arXiv.2503.01997
[84] E. Di Valentino, *et al.*, arXiv:2509.25288 (2025). https://doi.org/10.48550/arXiv.2509.25288
[85] I. Pantos, *et al.*, arXiv:2601.00650 (2026). https://doi.org/10.48550/arXiv.2601.00650
[86] A. G. Riess, *et al.*, Astrophys. J. Lett. **962**, L17 (2024). https://doi.org/10.3847/2041-8213/ad1ddd
[87] J. Simon, L. Verde, and R. Jimenez, Phys. Rev. D, **71**, 123001 (2005). https://doi.org/10.1103/PhysRevD.71.123001
[88] G.S. Sharov, and V.O. Vasiliev, Math. Model. Geom. **6**, 1-20 (2018). https://doi.org/10.26456/mmg/2018-611
[89] V. Sahni, *et al.*, JETP Lett. **77**, 201 (2003). https://doi.org/10.1134/1.1574831
[90] R. Caldwell and E. V. Linder, Phys. Rev. Lett. **95**, 141301 (2005). https://doi.org/10.1103/physrevlett.95.141301

ОБМЕЖЕНА ГОЛОГРАФІЧНА МОДЕЛЬ ТЕМНОЇ ЕНЕРГІЇ КАНІАДАКІСА В КОСМОЛОГІЇ БІАНЧІ *III*

Ю. Адитья[1*], **К. Дасунайду**[1**], **Мураласетті Ноокараджу**[2], **П. Сільпа**[3], **Г. Сурьянараяна**[4]

[1]*Кафедра математики, Технологічний інститут GMR (GMRIT) – Вважається університетом, Раджам-532127, Індія*

[2]*Кафедра хімії, Університет Адітья, Сурампалем-533437, Індія*

[3]*Кафедра хімії, Інженерний коледж Шрі Васаві, Тадепаллігудем-534101, Індія*

[4]*Кафедра математики, ANITS, Вішакхапатнам-533003, Індія*

У цій роботі ми вивчаємо космологічну динаміку анізотропного Всесвіту типу Біанкі–*III*, заповненого голографічною темною енергією Каньядакіса та матерією без тиску, в рамках теорії гравітації Бранса–Дікке–Расталла. Для отримання точних розв'язків рівнянь поля припускаються відповідні співвідношення між метричними потенціалами, а також функціональний зв'язок між скалярним полем та середнім масштабним коефіцієнтом. Для обмеження параметрів моделі ми виконуємо аналіз методом Монте-Карло за допомогою ланцюгів Маркова, використовуючи спільні набори даних CC+BAO. Реконструйований параметр Хаббла демонструє чудову відповідність зі спостережними даними в межах довірчих областей 1σ та 2σ, а оцінене значення постійної Хаббла узгоджується з останніми вимірюваннями. Ми виводимо кілька важливих космологічних параметрів, включаючи параметр Хаббла, параметр уповільнення, параметр рівняння стану, скалярне поле, космічний час та час ретроспективного огляду. Фізична поведінка цих параметрів аналізується за допомогою графічних зображень. Параметр уповільнення демонструє плавний перехід від ранньої фази уповільнення до пізньої прискореної фази, з червоним зміщенням переходу, що узгоджується з останніми спостережними межами. Параметр рівняння стану залишається у фантомній області, що вказує на динамічну поведінку темної енергії, здатну керувати поточним прискореним розширенням. Крім того, діагностика за допомогою методів пошуку станів (r, s) та (r, q) показує, що модель близько наближається до поведінки ΛCDM на пізніх етапах, допускаючи водночас відхилення на ранніх епохах. Діагностика $Om(z)$ додатково підтверджує фантомну природу темної енергії в сучасних рамках. Загалом, наші результати демонструють, що наша модель у гравітації Бранса-Дікке-Расталла забезпечує життєздатний та спостережливо узгоджений опис історії розширення космосу в анізотропному Всесвіті.

Ключові слова: *голографічна темна енергія Каньядакіса; гравітація Бранса-Дікке-Расталла; Всесвіт Біанкі III типу; аналіз МСМС; космічне прискорення*